COVID-19 scaling dynamics in growth and decline phases

Daniel Schertzer (Daniel.Schertzer@enpc.fr)
Ecole des Ponts ParisTech https://orcid.org/0000-0003-4930-5115
Ioulia Tchiguirinskaia (ioulia.tchiguirinskaia@enpc.fr)
Ecole des Ponts ParisTech https://orcid.org/0000-0002-0483-987X

Research Article

Keywords: Covid-19, epidemic dynamics, cascade of contacts, scale symmetry, growth and decline phases

Posted Date: November 12th, 2020

DOI: https://doi.org/10.21203/rs.3.rs-106550/v1

COVID-19 scaling dynamics in growth and decline phases

Daniel Schertzer*, Ioulia Tchiguirinskaia*
Hydrology Meteorology and Complexity Lab, Ecole des Ponts ParisTech, France

Abstract
The definition of optimal COVID-19 mitigation strategies remains worldwide on the top of public health agendas, particularly when facing a second wave. It requires a better understanding and a refined modelling of its dynamics. We emphasise the fact that epidemic models are phenomenologically based on the paradigm of a cascade of contacts that propagates infection. However, the introduction of ad-hoc characteristic times and corresponding rates spuriously break their scale symmetry.
Here we theoretically argue and empirically demonstrate that COVID-19 dynamics, during both growth and decline phases, is a cascade with a rather universal scale symmetry whose power-law statistics drastically differ from those of an exponential process. This involves slower but longer phases which are furthermore linked by a fairly simple symmetry. These results explain biases of epidemic models and help to improve them. Due to their generality, these results pave the way to a renewed approach to epidemics, and more generally to growth phenomena.

Introduction

The common root of most epidemics models is a cascade paradigm that can be traced back to their emergence with Bernoulli and d'Alembert[1], who preceded the celebrated quatrain of Richardson on the atmospheric dynamics cascade[2]. Indeed, their basic assumption is that each individual of the infected fraction I of a given population N will "on average" contaminate R_0 - the mythical "basic reproduction number"- individuals of the "susceptible" fraction S of this population. The complement to the fraction S is the population fraction $R = N\backslash S$ of the "removed" individuals, either having become immune or deceased, hence the acronym SIR for this type of models. Originally[3], these models were purely compartmental models, therefore with population fractions assumed to be homogeneous and the only variables are therefore their cumulative incidences $s(t)$, $i(t)$ and $r(t)$, usually driven by ordinary differential equations. Space inhomogeneity and resulting fluxes between different locations[4], as well as age dependencies[5] are now explicit in the current distributed epidemics models whose space time fields are driven by partial (integro-) differential equations.

At odd with cascade models developed in turbulence[6,7,8] and other domains[9], current epidemic models still rely on characteristic times that are assumed to be independent of the scale of observation, although there is no physical ground for this hypothesis. For instance, most epidemic models depend on or strive to estimate scale independent characteristic times T_c between contacts and T_r until recovery, whose ratio T_c/T_r, under strong homogeneity assumptions (e.g., uniform or Poisson distributions), yields a straightforward definition of the basic reproduction number R_0. These characteristic times have been implemented in various epidemic models[10] to obtain more elaborated estimates of an initial R_0 ranging from $2.06 - 2.52$ [11] to $3.6 - 4.0$ [12] and an "effective reproduction rate" $R \approx 4.08 \pm 0.36$ [13] for the COVID-19 pandemic. None of these studies tried to analyse the possible scale dependency of their estimates, whereas they admitted a sample dependency.

On the contrary, it is easy to point out that the time between contacts T_c sensitively depends on scale. Indeed, anyone would agree that the effective time between contacts t_c strongly depends on the mobility of the concerned agents, which has fluctuations over a wide range of space-time scales, e.g., from pedestrian walks to intercontinental flights. Not only recent epidemic models take a particular care to refine its representation, but the main goal and justification of the confinement strategies is to reduce the mobility nearly to zero[15,16,17,18]. Indeed, the intensification of mobility is suspected to have

led to qualitatively change the type of spread: from normal diffusion (e.g. for the Middle Age plague[19]) to anomalous diffusion. Normal diffusion does provide characteristic times due to the fact that the generating Gaussian distribution has a fall-off faster than an exponential (e.g., the probability to exceed 3 root mean squares (RMS) is only of the order of 10^{-5}, i.e., a Gaussian variable is never too far from the mean). For instance, the spread radius $\rho(t)$ can be measured by the RMS $\sigma(t)$ of particles emerging at the same time from the same source, which grows only like $t^{1/2}$, i.e. much slower than a ballistic diffusion ($\rho(t) \approx t$). On the contrary, anomalous diffusion is generated by Levy stable distributions that are devoid of characteristic times due to their power-law fall-off , i.e., the probability to exceed a distance $\rho(t)$ on a given time falls off as $\rho(t)^{-(1+\alpha)}$, with $0 < \alpha < 2$ [20, 21]. As a consequence, the RMS $\sigma(t)$ does not exist. Furthermore, the probability to exceed c times a given distance $\rho(t)$ decreases only by the factor $c^{-\alpha}$, which shows that we can easily be far away from the mean… which furthermore exists only for $\alpha > 1$! Such anomalous diffusion due to human mobility has received some empirical support from a large scale experiment ironically nicknamed "where is George". This experiment corresponds to first tracking via an internet site, over ten millions of displacements of about half a million of one dollar bills (bearing the image of George Washington) then to analyse them[22]. The important result obtained was that this diffusion was anomalous and nearly isotropic in space and time with a common exponent $\alpha \approx 0.6$. It therefore corresponds to a strong super diffusivity. It was also shown that a random walker in a Chernobyl contaminated field accumulates radiation doses that also anomalously fluctuate, contrasting sharply with the usual average estimates[23]. Refined small scales statistics of time between contacts could be obtained with the deployment of mobile tracking applications, which nevertheless should protect privacy[24]. Another important aspect to be taken into account is the fractality of measuring networks[25].

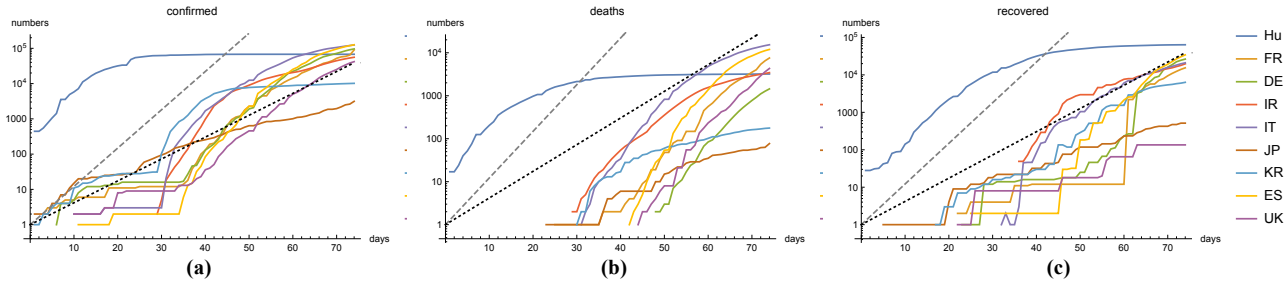

Fig.1: Sub-exponential growth phase: log-linear plots of **(a)** confirmed, **(b)** death, **(c)** recovered cumulative incidences $X(t)$ of the following entities: Hubei, France, Germany, Iran, Italy, Japan, Korea, Spain and United Kingdom, over the period 22 January - 04 April. An exponential behaviour would correspond to straight lines like those drawn for characteristic times $T = 4;7$ days, and therefore to doubling times $T_2 = T\ln(2) \approx 3;5$ days (respectively dashed grey and dotted black straight lines). Due to their (strong) concavity, all the trajectories are sub-exponentials, i.e., grow slower than any of their local approximations by an exponential that corresponds to a tangent to these log-linear graphs.

Characteristic times T and the corresponding "doubling times" T_2 are related to differential equations of the type:

$$dX/dt \approx X(t)/T; T_2 = T\ln(2) \quad (1)$$

and their exponential solution $X(t) \approx X(t_0)\exp((t-t_0)/T)$, where the symbol $\approx$ denotes an equivalence that can be more general than a strict deterministic equality, e.g., asymptotic equivalence on a given range of times or/and up to a slowly varying factor, or/and an equality in probability distribution, etc.. The SIR model provides again a rather simple example of this behaviour. For a constant population ($s(t) + i(t) + r(t) = n(t) = n = const$) it yields the following evolution equation for the infected population:

$$di(t)/dt \approx (R_0 s(t)/n - 1)i(t)/T_c \approx (R_0 s(0)/n - 1)i(t)/T_c \quad (2)$$

The second r.h.s. approximation is valid during the initial outbreak ($s(t) \approx s(0)$), whereas the awaited "flattening of the epidemic wave" ($\frac{di(t)}{dt} = 0$) occurs in the SIR model only when the susceptible population $s(t)$ has been significantly reduced with respect to the total population n, hence it occurs at the time s_f such that: $s(t_f)/n = R_0^{-1}$ or $(i(t_f) + r(t_f))/n = 1 - R_0^{-1}$.

Database

We will not discuss either the interests (e.g., analytically solvable[3]) or limitations (e.g., non-accounted spatial and intra-compartmental heterogeneities) of the SIR model that we only used to introduce basic concepts needed to explore the database of the Center for Systems Science and Engineering at Johns Hopkins University[26], more precisely its convenient github web site https://github.com/CSSEGISandData/COVID-19/tree/master/csse_covid_19_data. This database provides daily estimates of the "confirmed", "deaths" and "recovered" cumulative incidences for 187 countries. These data are refined for some regions, e.g.: the data on China are distributed according to all the provinces, metropolitan France is distinct from the overseas departments and the American data are provided according to 3261 urban agglomerations and dependencies.

For presentation clarity, results are only displayed for the following entities: Hubei, France, Germany, Iran, Italy, Japan, Korea, Spain and United Kingdom. The choice of these time series is based on their length, as well as their relative high counts. Both factors could presumably reduce artefacts such as incomplete counts or even possible offsets for various reasons, including political ones. However, important changes in tests or/and count methodologies or simply data transmission delays did introduce non negligible, artificial fluctuations in theses series. For instance, important changes on COVID-19 infection evaluations such as $+15100$ in the Hubei province occurred on 13 February and $+26800$ in France on 12 April. An additional cumulation of 325 cases in the Hubei province was added to the datasets on ad-hoc dates, a month later the official ending of the epidemic spread in this area. Often, the deaths in rest homes began to be included only at a later stage of the epidemic. Furthermore, data were not always daily provided, therefore introducing a zero increment between two consecutive days, followed by an artificially enlarged increment for the second day. However, our data analysis is rather robust with respect to this sort of time translation, contrary to the direct analysis of the time evolution of the cumulative incidence $X(t)$. There are other disrupting examples of data adjustments, such as the cumulation of the "deaths" incidences was decreased by 1918 cases in Spain on 25 May.

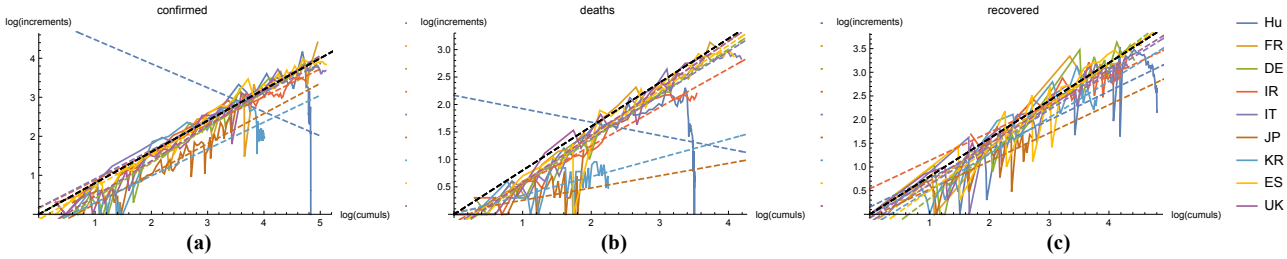

Fig.2: Cumulative-incremental analysis of the growth phase: log-log plots of the couples $(X(t), \Delta X(t))$, where $\Delta X(t) = X(t) - X(t - \Delta t))$ is the increment (the time increment Δt being one day) of **(a)** "confirmed", **(b)** "deaths", **(c)** "recovered" cumulative incidence $X(t)$ of the following entities: Hubei, France, Germany, Iran, Italy, Japan, Korea, Spain and United Kingdom, over the period 22 January- 04 April. Graphs should be read from left to right to follow the time arrow ($X(t)$ being non decreasing with time) and the almost vertical parts on the right-hand side corresponds to compressed views of decline phases to be expanded in Fig.3.
These graphs display a rather universal behaviour, especially a common scaling/power-law behaviour $\Delta X(t_i) \approx aX(t_i)^b$, a discrete version of the differential equation Eq. 4, over a non negligible range of couples $(X(t), \Delta X(t))$ and therefore of time, with only a few exceptions. The best linear fits are represented by the dashed lines (of the same colour as the graph of this entity), with high determination coefficients R^2 and limited dispersion of the estimates of the feedback exponent b (see Supplementary Information). The black dashed line indicates the average estimates over the period of 22 January - 04 April.

However other entities, and other epidemic data as well, display similar graphs that have called attention to power-law growth, including with the help of log-log curve fittings[27, 28, 29]. But, these fits are sensitive to the choice of the initial time and data artefacts. We therefore developed a specific data analysis presented below.

We analysed data from 22 January till 07 June hence containing both the end of the crisis in Hubei and its beginning in Europe to enable to analyse both stages of the epidemic. Two intermediate dates were used for a comparative analysis: 4 April as a tentative date for the well-advanced growth phase in Europe (about 3 weeks after the pandemic announcement by WHO), and 16 April as the ending date of the epidemic for the Hubei province). Nevertheless, tentative explorations until the beginning of November have confirmed the interest of a follow-up paper focused on the beginning of the second wave.

Growth phase analysis

Figure 1 shows that the time evolution of the cumulative incidence $X(t)$ of the aforementioned categories and entities are sub-exponential. Hence, we introduce a scaling dependency (i.e. a power-law) of their characteristic times $T(t)$ (and doubling time $T_2(t)$) with respect to the current scale $X(t)$:

$$T(t) \approx X(t)^{1-b}/a;\ T_2(t) \approx \ln(2) X(t)^{1-b}/a \quad (3)$$

where the exponent b can be close to unity, but nevertheless distinct of it, and the prefactor a is no longer the inverse of a (characteristic) time except for $b = 1$. The presence of the prefactor $X(t)^{1-b}$ in the local time $T(t)$ (for $b \neq 1$ in Eq. 3) makes all the difference (except at the initial time t_0 of the contamination $X(t_0) = 1$) with respect to the exceptional case $b = 1$ (Eq.1): the local times $T(t)$ and $T_2(t)$ are no longer invariants of the contamination dynamics, but increase with t (for $b < 1$). This merely corresponds to the fact that the system became less and less efficient due to its larger and larger outer scale, which rather makes sense. As expected, this increase of $T(t)$ yields a slower growth of $X(t)$ with respect to the exponential model.

Injecting the time $T(t)$ in Eq.1 yields its scaling generalisation:

$$dX/dt \approx aX(t)^b \quad (4)$$

where b can be now be understood as the feedback exponent from the cumulative incidence $X(t)$ onto the elementary increment $dX(t) = X(t) - X(t - dt)$, both are thus non stationary. This is a common feature for growth processes [29], but not for cascades, which are usually supposed to have a stationary outer scale. We therefore need to proceed to a "cumulative-incremental analysis" to quantify this feedback, mainly to determine its exponent b. The simplicity of this analysis might help to change the human behaviour with respect to epidemic risks, whose importance has been often underlined[14].

The very first step (see Fig.2) corresponds to simply graph $\Delta X(t_i)$ vs. $X(t_i)$ in a log-log plot, where $\Delta X(t_i) = X(t_i) - X(t_{i-1})$. It is rather surprising to see how much the curves (corresponding to the various entities recalled above) collapse together providing a first indication of a given universality of the virus dynamics over a range of time scales (see Supplementary Information). Furthermore, the range over which this universality is better observed corresponds to power-laws $\Delta X(t_i) \approx aX(t_i)^b$, i.e., a discrete versions of Eq.3. This scaling behaviour is supported by least square fits of the cumulative-incremental incidence curves (dashed straight lines in the log-log plot of Fig.2) with high determination coefficients R^2 and limited dispersion of the estimates throughout the time scales (see Supplementary Information).

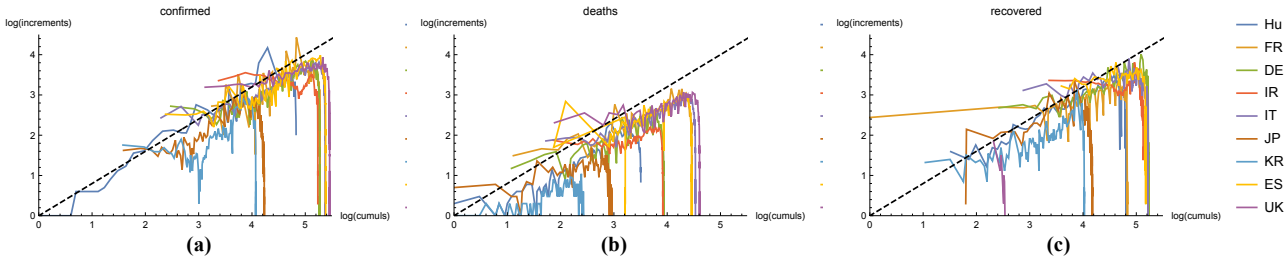

Fig.3: Cumulative-incremental analysis of the decline phase: log-log plots of the couples $(X_{max} - X(t), \Delta X(t))$ to analyse the decline phase of **(a)** confirmed, **(b)** deaths, **(c)** recovered incidences cumulative $X(t)$ of the aforementioned entities (Hubei, France, Germany, Iran, Italy, Japan, Korea, Spain and United Kingdom), over the period 22 January – 07 June, with an exception of shorter period for Hubei till 16 April. Contrary to those of Fig.2, these graphs should be read from right to left to follow the time arrow ($X_{max} - X(t)$ being non increasing with time) and the almost vertical parts on the right hand side corresponds to compressed views of growth phases, which were expanded in Fig.2.

The reference curve (dashed black straight line) corresponds to the equation $\Delta X(t) = (X_{max} - X(t))^{\bar{b}}$, where $\bar{b}$ denotes the average value of the feedback exponents b's of the growth phase analysis (Fig.2). Hubei (dark blue) and Korea (light blue) rather clearly confirm a feedback exponent $b' \approx \bar{b}$, while other time series were beginning their decline phase. The loop exhibited by the time series of Spain in the category "deaths" is due to a sharp decrease (-1918 cases) of this cumulation on 25 May. All the posterior daily cumulation remain inferior to the cumulation of 24 May. There are similar behaviours, although less obvious due to smaller adjustments, for some other countries.

The most important result is that the estimates of the feedback exponent b are clearly below 1 for all types of time series over the period 22 January to 04 April: 0.81 ± 0.09 (confirmed cases), 0.68 ± 0.25 (deaths), 0.78 ± 0.13 (recovered). These estimates are mainly obtained on growth phases, however as displayed by Fig.3, their mean values fit rather well the corresponding decline phases (see Supplementary Information).

The local time $T(t)$ (Eq.3) increases linearly with respect to time, with the prefactor $(1 - b)$. Indeed, a straightforward integration of Eq.4 yields:

$$\forall t_1, t_2 \colon\ t_2 - t_1 = (X(t_2)^{1-b} - X(t_1)^{1-b})/(a(1-b)) = (T(t_2) - T(t_1))/(1-b) \qquad (5)$$

The empirical, local times $T(t)$ (defined by Eq.3 and normalised by $(1 - b)$) are in agreement with this relation in the growth phase (see Supplementary Information).

Decline phase analysis

The second stage of the cumulative-incremental analysis is to explore the decline phase. By reversing the process $X(t)$ from its maximal value $X_{max} = X(t_{max})$, we obtain a process $X'(t')$:

$$X'(t') = X_{max} - X(t);\ t' = t_{max} - t \qquad (6)$$

whose growth phase corresponds to the decline phase of $X(t)$ and vice-versa. As $dX/dt = dX'/dt'$, the scaling decline phase is ruled by a slight modification of Eq.4:

$$dX/dt \approx a'(X_{max} - X(t))^{b'} \qquad (7)$$

Thanks to this symmetry, the cumulative-incremental analysis remains rather the same: it analyses the (discrete) graph $\Delta X(t_i)$ vs. $(X_{max} - X(t_i))$, seeking a power law relation for large times t_i's. Figure 3 shows an overall agreement with $b' \approx b$, particularly for the Hubei province that has a fully developed decline phase. For other countries the total cumulation is weakly approached by the empirical X_{max}, resulting in a temporary flattening of last points (see Supplementary Information).

Discussion and conclusions

So far, we have been using only deterministic calculus, whereas Figs. 2, 3 display non negligible fluctuations with respect to a power-law. Not all of these fluctuations result either from data

uncertainty, or from quasi-Gaussian perturbations. These deviations can be easily accounted for in the framework of stochastic multiplicative cascades[30]. These processes are exponentials of a stochastic generators $\Gamma(t)$ that broadly generalise $\ln(t - t_0)/(b - 1)$. However, their stochastic differentiation remains rather close to the deterministic one, mostly adding a supplementary term σdt to the differential of the generator:

$$dX(t) \approx X(t)\, d\Gamma(t) + \sigma\, dt \quad (8)$$

When the generator $\Gamma(t)$ is Gaussian, σ is the "quadratic variation", extensions to Lévy stable generators, which are strongly non-Gaussian, have been also considered[8].

Therefore, the next stage of the cumulative-incremental analysis is to investigate the stochastic nature of the cascade generator, as well as how it respects the aforementioned symmetry between the growth and decline phases (Eq. 6). Universal multifractals[30] can provide some preliminary, universal scaling characterisation, despite the present sample limitations (see Supplementary Information). The present results paved the way for joint scaling analysis of the vector-valued time series $(X_1(t), X_2(t), X_3(t))$, instead of separately analysing the time series corresponding to the three categories, and to introduce location and other dependencies. This would correspond to enlarge the domain, on which the process and its generator are defined, as well as their co-domain, on which they are valued[8].

References

1. Dietz, K. & Heesterbeek, J. A. P. Bernoulli was ahead of modern epidemiology. *Nature* 513–514 (2000).
2. Richardson, L. F. *Weather prediction by numerical process*. (Cambridge University Press republished by Dover, 1965, 1922).http://www.nature.com/nphys/
3. Kermack, W. O. & McKendrick, A. G. A Contribution to the Mathematical Theory of Epidemics. *Proc. R. Soc. A* 700–721 (1927). doi:10.1098/rspa.1927.0118
4. Sander, L. M., Warren, C. P., Sokolov, I., Simon, C. & Koopman, J. Percolation on disordered networks as a model for epidemics. *Math. Biosci* **180**, 293–305 (2002).
5. Pellis, L., Cauchemez, S., Ferguson, N. M. & Fraser, C. epidemic predictions. *Nat. Commun.* 906 (2020). doi:10.1038/s41467-019-14229-4
6. Monin, A. S. & Yaglom, A. M. *Statistical Fluid Mechanics*. (MIT press, 1975).
7. Frisch, U. *Turbulence: The Legacy of A. N. Kolmogorov*. (Cambridge University Press, 1995).
8. Schertzer, D. & Tchiguirinskaia, I. A century of turbulent cascades and the emergence of multifractal operators. *Earth Sp. Sci.* **7**, e2019EA000608 (2020).
9. Ghashghaie, S. *et al.* Turbulent cascades in foreign exchange markets. *Nature* **381**, 767–770 (1996).
10. Castillo-Chavez, C., Feng, Z. & Huang, W. On the computation of R0 and its role on global stability. in *Mathematical approaches for emerging and reemerging infectious diseases: an introduction.* (eds. Castillo-Chavez, C., Blower, S., van den Driessche, P., Kirschner, D. & Yakubu, A.) 229–250 (Springer, 2002).
11. Zhang, S. *et al.* Estimation of the reproductive number of novel coronavirus (COVID-19) and the probable outbreak size on the Diamond Princess cruise ship : A data-driven analysis. *Int. J. Infect. Dis.* **93**, 201–204 (2020).
12. Read, J. M., Bridgen, J. R. E., Cummings, D. A. T., Ho, A. & Jewell, C. P. Novel coronavirus 2019-nCoV: early estimation of epidemiological parameters and epidemic predictions. *medRxiv prepr* 1–11 (2020). doi:10.1101/2020.01.23.20018549
13. Cao, Z. *et al.* Effective reproduction number of 2019-nCoV. *medRxiv Prepr.* (2020). doi:10.1101/2020.01.27.20018952
14. Ferguson, N. Capturing human behaviour. *Nature* **446**, 733 (2007).
15. Ferguson, N. M. *et al.* Strategies for mitigating an influenza pandemic. *Nature* **442**, 448–452 (2006).
16. Flahault, A., Ferguson, N. M., Cauchemez, S., Valleron, A. & Boe, P. Estimating the impact of school closure on influenza transmission from Sentinel data. *Nature* **452**, 6–11 (2008).
17. Chinazzi, M. *et al.* The effect of travel restrictions on the spread of the 2019 novel coronavirus (COVID-19) outbreak. *Science (80-.).* 9757 (2020). doi:10.1126/science.aba9757
18. Neil M Ferguson, N. M. *et al.* COVID-19 reports | Faculty of Medicine | Imperial College London. 20 (2020). doi:https://doi.org/10.25561/77482
19. Christakos, G., Olea, R. A., Serre, M. L., Yu, H.-L. & Wang, L.-L. *Interdisciplinary Public Health Reasoning and Epidemic Modelling: The Case of Black Death*. (Springer-Verlag, 2005).
20. Feller, W. *An Introduction to probability theory and its applications, vol. 2*. (Wiley, 1971).
21. Schertzer, D., Larchevêque, M., Duan, J., Yanovsky, V. V & Lovejoy, S. Fractional Fokker--Planck Equation for Nonlinear Stochastic Differential Equations Driven by Non-Gaussian Levy Stable Noises. *J. Math. Phys.* **42**, 200 (2004).
22. Brockmann, D., Hufnagel, L. & Geisel, T. The scaling laws of human travel. *Nature* **439**, 462–465 (2006).

23. Tchiguirinskaia, I., Schertzer, D., Hubert, P., Bendjoudi, H. & Lovejoy, S. Multiscaling geophysics and sustainable development. in *Scales in Hydrology and Water Management* (eds. Tchiguirinskaia, I., Bonnel, M. & Hubert, P.) **287**, 111–136 (IAHS Press, 2004).
24. Cho, H., Ippolito, D. & Yu, Y. W. Contact Tracing Mobile Apps for COVID-19: Privacy Considerations and Related Trade-offs. *ArXiv Prepr.* (2020).
25. Lovejoy, S., Schertzer, D. & Ladoy, P. Fractal characterisation of inhomogeneous measuring networks. *Nature* **319**, 43–44 (1986).
26. Dong, E., Du, H. & Gardner, L. COVID-19 in real time. *Lancet Infect. Dis.* **3099**, 19–20 (2020).
27. Manchein, C., Brugnago, E. L., Silva, R. M., Mendes, C. F. O. & Marcus, W. Strong correlations between power-law growth of COVID-19 in four continents and the inefficiency of soft quarantine strategies. *Chaos* **30**, 041102 (2020).
28. Maie, B. F. & Brockman, D. Effective containment explains sub-exponential growth in confirmed cases of recent COVID-19 outbreak in Mainland China. *ArXiv Prepr.* (2020).
29. Chowell, G., Viboud, C., Simonsen, L. & Moghadas, S. M. Characterizing the reproduction number of epidemics with early subexponential growth dynamics. *J. R. Soc. Interface* **13**, 20160659 (2016).
30. Schertzer, D. & Lovejoy, S. Physical modeling and analysis of rain and clouds by anisotropic scaling multiplicative processes. *J. Geophys. Res.* **92**, 9693–9714 (1987).

Supplementary Information

is linked to the online version of the paper at https://www.nature.com/.

Acknowledgments

This work is supported by the Academic Chair "Hydrology for Resilient Cities" of Ecole des Ponts ParisTech, endowed by Veolia.

Author contributions

Both authors equally contributed to the paper and therefore the alphabetical order is used.

Conflict of interest

There is no conflict of interest

Data and results duplication

As explained in the text, only the open data of the Center for Systems Science and Engineering at Johns Hopkins University have been used (https://github.com/CSSEGISandData/COVID-19/tree/master/csse_covid_19_data). Furthermore, authors are willing to provide on request the standalone Mathematica program that was used to perform these analyses and to generate a large number of figures, from which were selected the few presently presented in this paper and its Supplementary Information.

Figures

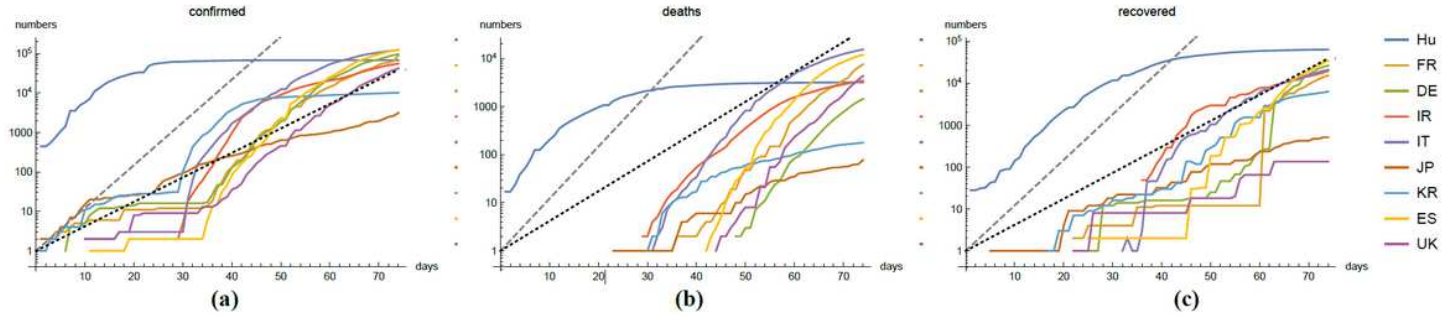

Figure 1

Sub-exponential growth phase: log-linear plots of (a) confirmed, (b) death, (c) recovered cumulative incidences □(□) of the following entities: Hubei, France, Germany, Iran, Italy, Japan, Korea, Spain and United Kingdom, over the period 22 January - 04 April. An exponential behaviour would correspond to straight lines like those drawn for characteristic times □ = 4; 7 days, and therefore to doubling times □ = □ ln(2) ≈ 3; 5 days (respectively dashed grey and dotted black straight lines). Due to their (strong) concavity, all the trajectories are sub-exponentials, i.e., grow slower than any of their local approximations by an exponential that corresponds to a tangent to these log-linear graphs.

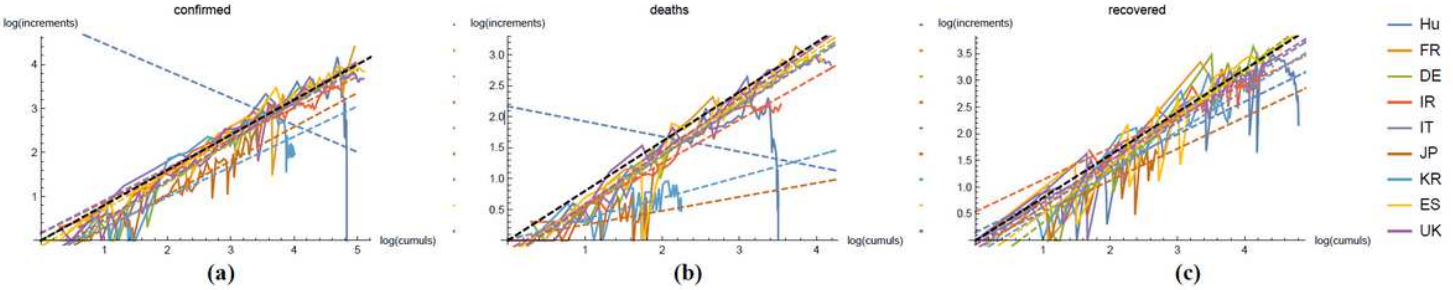

Figure 2

Cumulative-incremental analysis of the growth phase: log-log plots of the couples (□(□), Δ□(□)), where Δ□(□) = □(□) − □(□ − Δ□)) is the increment (the time increment Δ□ being one day) of (a) “confirmed”, (b) “deaths”, (c) “recovered” cumulative incidence □(□) of the following entities: Hubei, France, Germany, Iran, Italy, Japan, Korea, Spain and United Kingdom, over the period 22 January- 04 April. Graphs should be read from left to right to follow the time arrow (□(□) being non decreasing with time) and the almost vertical parts on the righthand side corresponds to compressed views of decline phases to be expanded in Fig.3. These graphs display a rather universal behaviour, especially a common scaling/power-law behaviour Δ□(□i) ≈ □□(□i)□, a discrete version of the differential equation Eq. 4, over a non negligible range of couples (□(□), Δ□(□)) and therefore of time, with only a few exceptions. The best linear fits are represented by the dashed lines (of the same colour as the graph of this entity), with high determination coefficients □2 and limited dispersion of the estimates of the feedback exponent □ (see Supplementary

Information). The black dashed line indicates the average estimates over the period of 22 January - 04 April.

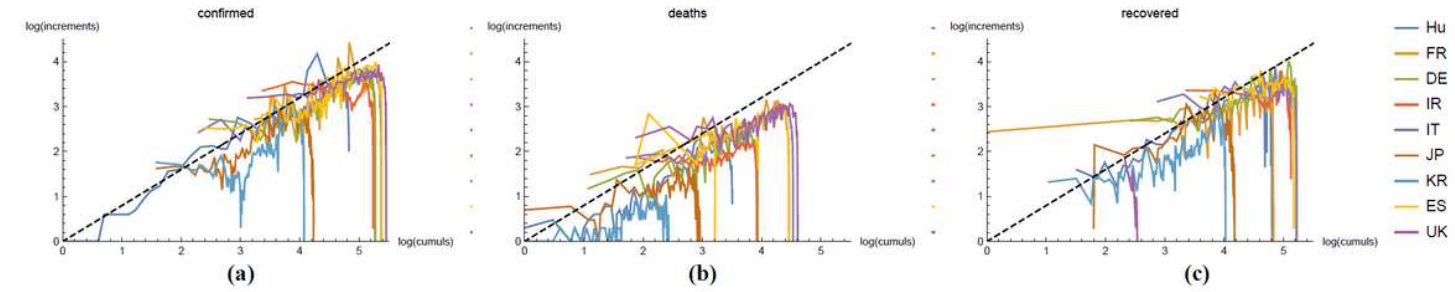

Figure 3

Cumulative-incremental analysis of the decline phase: log-log plots of the couples (□max − □(□), Δ□(□)) to analyse the decline phase of (a) confirmed, (b) deaths, (c) recovered incidences cumulative X(t) of the aforementioned entities (Hubei, France, Germany, Iran, Italy, Japan, Korea, Spain and United Kingdom), over the period 22 January – 07 June, with an exception of shorter period for Hubei till 16 April. Contrary to those of Fig.2, these graphs should be read from right to left to follow the time arrow (□max − □(□) being non increasing with time) and the almost vertical parts on the right hand side corresponds to compressed views of growth phases, which were expanded in Fig.2. The reference curve (dashed black straight line) corresponds to the equation Δ□(□) = (□max − □(□))□ , where □ denotes the average value of the feedback exponents □'s of the growth phase analysis (Fig.2). Hubei (dark blue) and Korea (light blue) rather clearly confirm a feedback exponent □' ≈□, while other time series were beginning their decline phase. The loop exhibited by the time series of Spain in the category “deaths" is due to a sharp decrease (−1918 cases) of this cumulation on 25 May. All the posterior daily cumulation remain inferior to the cumulation of 24 May. There are similar behaviours, although less obvious due to smaller adjustments, for some other countries.

Supplementary Files

This is a list of supplementary files associated with this preprint. Click to download.

- COVID19cascadeSupplementaryInformation20201106.pdf